



Advanced diffusion-weighted MRI models for preoperative prediction of lymph node metastasis in resectable gastric cancer

Jing Li¹ · Hongkai Zhang¹ · Tianxia Bei¹ · Yi Wang¹ · Fei Ma¹ · Shaoyu Wang² · Haocheng Li³ · Jinrong Qu¹

Received: 18 July 2024 / Revised: 20 August 2024 / Accepted: 29 August 2024
© The Author(s), under exclusive licence to Springer Science+Business Media, LLC, part of Springer Nature 2024

Abstract

Objective To investigate the potential of six advanced diffusion-weighted imaging (DWI) models for preoperative prediction of lymph node metastasis (LNM) in resectable gastric cancer (GC).

Methods Between Nov 2022 and Nov 2023, standard MRI scans were prospectively performed in consecutive patients with endoscopic pathology-confirmed gastric adenocarcinoma who were referred for direct radical gastrectomy. Six DWI models, including fractional order calculus (FROC), continuous-time random walk (CTRW), diffusion kurtosis imaging (DKI), intravoxel incoherent motion (IVIM), the mono-exponential model (MEM) and the stretched exponential model (SEM) were computed. Surgical pathologic diagnosis of LNM was the reference standard, and patients were classified into LNM-positive or LNM-negative groups accordingly. The morphological features and quantitative parameters of the DWI models in different LNM categories were analyzed and compared. Multivariable logistic regression was used to screen significant predictors. Receiver-operating characteristic curves and the area under the curve (AUC) were plotted to evaluate the performances, the Delong test was performed to compare the AUCs.

Results In the LNM-positive group, tumor thickness and kurtosis (DKI_K) were significantly higher, while anomalous diffusion coefficient (CTRW_D), diffusivity (DKI_D), diffusion coefficient (FROC_D), pseudodiffusion coefficient (IVIM_D*), perfusion fraction (IVIM_f), and ADC were lower compared to the LNM-negative group. Clinical tumor staging (cT) and CTRW_D were independent predictors. Their combination demonstrated a superior AUC of 0.930, significantly higher than that of individual parameters.

Conclusions Tumor thickness, DKI_K, CTRW_D, DKI_D, FROC_D, IVIM_D*, IVIM_f and ADC were associated with LNM status. The combination of independent predictors of cT and CTRW_D further enhanced the performance.

Keywords Diffusion-weighted magnetic resonance imaging · Stomach neoplasms · Lymph node metastasis

✉ Jing Li
lijingqingqing@163.com

✉ Jinrong Qu
qjryq@126.com

Hongkai Zhang
zhanghkcancer@163.com

Tianxia Bei
beitianxia@163.com

Yi Wang
wyft1022@163.com

Fei Ma
mafeizzu@outlook.com

Shaoyu Wang
shaoyu.wang@siemens-healthineers.com

Haocheng Li
lhc20010321@163.com

- 1 The Affiliated Cancer Hospital of Zhengzhou University & Henan Cancer Hospital, Zhengzhou, China
- 2 MR Research Collaboration, Siemens Healthineers, Shanghai, China
- 3 Sanquan College of Xinxiang Medical University, Xinxiang, China

Abbreviations

ADC	Apparent diffusion coefficient
cT	Clinical stage
CTRW	Continuous-time random walk diffusion-weighted imaging
CTRW _α	Temporal diffusion heterogeneity
CTRW _β	Spatial diffusion heterogeneity
CTRW _D	Anomalous diffusion coefficient
DKI	Diffusion kurtosis imaging
DKI _D	Diffusivity
DKI _K	Kurtosis
DWI	Diffusion weighted imaging
FROC	Fractional order calculus diffusion
FROC _D	Diffusion coefficient
FROC _β	Intravoxel diffusion heterogeneity parameter
FROC _μ	Spatial parameter
GC	Gastric cancer
IVIM	Intravoxel incoherent motion diffusion-weighted imaging
IVIM _D	True diffusion coefficient
IVIM _D *	Pseudodiffusion coefficient
IVIM _f	Pseudodiffusion fraction
LNM	Lymph node metastasis
MRI	Magnetic resonance imaging
SEM	Stretched exponential model
SEM _α	Water diffusion heterogeneity index
SEM _{DDC}	Distributed diffusion coefficient

Introduction

Gastric cancer (GC) was the fifth most frequently diagnosed cancer and the fifth leading cause of cancer death in 2022 [1]. Precise staging, particularly regarding lymph node metastasis (LNM), is essential for treatment planning and prognosis [2–4]. LNM status dictates treatment options, such as contraindicating endoscopic mucosal resection for early GC and indicating neoadjuvant therapy for locally advanced cases [3, 4]. Additionally, LNM significantly impacts patient survival and disease progression [5–7]. Current preoperative diagnosis of LNM primarily relies on imaging-based assessment, with computed tomography (CT) being the recommended modality [8, 9]. However, the performance of CT in predicting LNM varies markedly [10–12]. Positron emission tomography has been used for staging of GC, but no significantly added benefit has been reported in detecting positive nodes in esophago-gastric cancer or GC [13, 14]. Functional magnetic resonance imaging, particularly diffusion weighted imaging (DWI), has shown additional value in the staging of GC [15, 16]. However, in mono-exponential model of DWI, water molecular motion is simulated to follow a Gaussian distribution which is not the case in

heterogeneous cancerous tissue [17]. Emerging advanced DWI models, such as diffusion kurtosis imaging (DKI), stretched-exponential models (SEM), intravoxel incoherent motion (IVIM), the fractional order calculus (FROC) model and continuous-time random walk (CTRW) model are increasingly utilized to depict authentic water motion in vivo and tumor heterogeneity in the microenvironment [18–24], and offer new sets of imaging markers for cancers. Regarding GC, the true diffusion coefficient of IVIM is a useful index for evaluating LNM and lymphovascular invasion [19, 25]. The kurtosis of DKI is positively correlated with Ki-67 expression and useful for evaluating treatment response [18, 26]. The FROC model provides useful tools for noninvasive assessment of the Lauren classification [27]. These studies together highlight the promise of advanced DWI models in the stomach. We postulated that advanced DWI models with additional novel imaging markers can provide multiple perspectives into tumor characteristics, which may assist more accurate preoperative prediction of LNM among GC patients. Therefore, the aim of this study was to investigate the potential and added value of six DWI models (mono-exponential DWI, IVIM, SEM, DIK, FROC, and CTRW) for preoperative prediction of LNM in patients with resectable GC.

Methods

Patients

The present prospective study received approval from our hospital's institutional review board and adhered to the principles of the Declaration of Helsinki. All participants provided written informed consent (NCT04028375). Between Nov 2022 and Nov 2023, patients diagnosed with gastric adenocarcinoma by endoscopic biopsy were enrolled following the inclusion criteria as: (a) had no history of prior anticancer treatment or any concurrent malignancy; (b) had completed gastric MRI scans before surgery; and (c) had resectable GC lesions (cT1–4a, N0–1, M0) assessed by the multidisciplinary tumor board (MDT) and scheduled direct radical gastrectomy. Patients were excluded if (a) postoperative pathology confirmed as mucinous adenocarcinomas because its mucinous nature may cause migrations of ADC values; (b) had the tumor diameter < 10 mm, which was insufficient to place a valid region of interest (ROI); or (c) had low-quality images (image score < 3). The flowchart for patient recruitment is displayed in Fig. 1. The framework of MDT for evaluating tumor resectability is shown in Figure S1, Supplementary Materials.

Fig. 1 The flowchart of patient recruitment

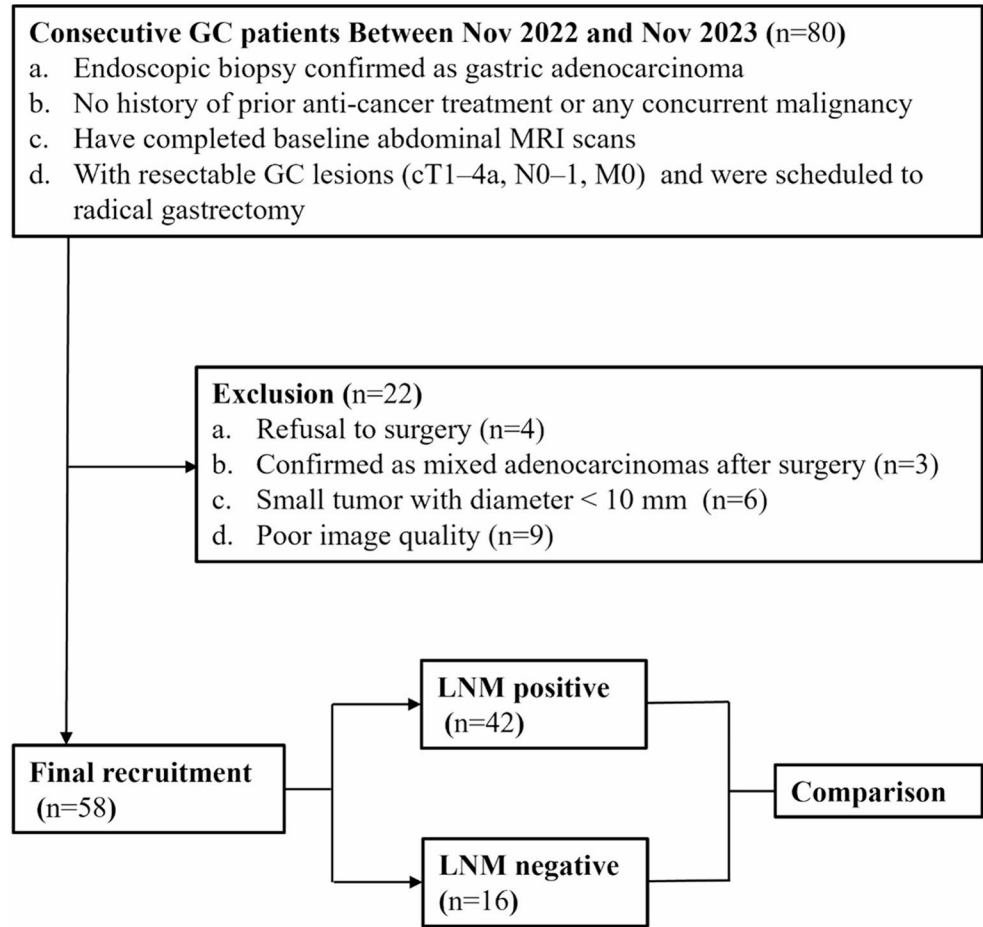


Table 1 MRI acquisition protocol

Parameters	T1WI axial	T2WI axial	Multi-b value DWI sequence (b = 0, 25, 50, 75, 100, 200, 400, 800, 1200, 1600, 2400, 3000 s/mm ²)
TR (ms)	3.9	4500~7800	8000
TE (ms)	1.32/2.74	98	59
Slice thickness (mm)	5	5	5
Slice gap (mm)	NA	0.5	0.5
NEX	1	2	1~4
FOV (cm ²)	38×38	28.7×28.7	38×38
Resolution	180×288	193×384	83×128
Voxel size (mm ³)	1.47×1.32×4.23	1.49×1.04×5	3.28×2.66×5
Flip angle (°)	9	120	NA

Abbreviations TR = Repetition time; TE = Echo time; NEX = Number of excitations, FOV = Field of view. Note: NEX for IVIM range from 1–4, NEX = 1 for b = 0, 25, 50, 75, 100, 200, 400 s/mm², NEX = 2 for b = 800 s/mm², NEX = 3 for b = 1200 s/mm², NEX = 4 for b = 1600, 2400, 3000 s/mm²

MRI protocol

All participants underwent gastric MRI scans within one week before surgery (median: 3 days) using a 3.0 T MR scanner (MAGNETOM Prisma, Siemens Healthineers) equipped with an anterior 18-element body coil and an integrated posterior 32-element spine coil array. After 6 h of fasting, each patient was trained to breathe rhythmically to reduce unwanted respiratory motion artifacts, and was

instructed to consume 500 mL of warm water 10 min in advance to distend the stomach. Thereafter, raceanisodamine hydrochloride (10 mg) was intramuscularly administered within 15 min before MRI acquisition. Table 1 presents the standard protocol with detailed acquisition parameters, including (a) 3D volumetric interpolated breath-hold examination (VIBE) axial T1WI. (b) Axial respiratory-triggered, fat-suppressed turbo spin echo (fs_TSE) T2WI. (c) Multi-b value DWI obtained using echo planar imaging-based the

prototyped integrated specific slice dynamic Shim (iShim) sequence. With the aforementioned sequences, 2D multi-gradient echo images were initially acquired for each imaging slice. The orientation and field of view (FOV) for these images were adjusted based on the corresponding imaging slices. Subsequently, we distinguished fat and water by analyzing the difference in echo time between the first and last echoes. Following this, a phase difference image was computed from the two echoes, and 12 b values were applied within the range of 0–3000 s/mm² (0, 25, 50, 75, 100, 200, 400, 800, 1200, 1600, 2400, 3000 s/mm²) [28]. The diffusion gradient parameters included a gradient amplitude (G) of 80 mT/m, diffusion gradient duration (δ) of 11.1 ms, time separation between two diffusion gradient lobes (Δ) of 23.9 ms, and a total acquisition time of 3 min and 40 s.

Diffusion models reconstruction

A domestic BoDiLab software was used to process the raw multi-b value DWI data to generate parametric maps by fitting six DWI models, including CTRW, DKI, FROC, IVIM, SEM, and conventional mono-exponential model. These sequences generated 14 parameters, including temporal diffusion heterogeneity (CTRW_ α), spatial diffusion heterogeneity (CTRW_ β), and anomalous diffusion coefficient (CTRW_D) from CTRW, diffusivity (DKI_D) and kurtosis (DKI_K) from DKI; the anomalous diffusion coefficient (FROC_D), intravoxel diffusion heterogeneity parameter (FROC_ β), and spatial parameter (FROC_ μ) from FROC; the true diffusion coefficient (IVIM_D), the pseudodiffusion coefficient (IVIM_D*) and the perfusion

fraction (IVIM_f) from IVIM; the water diffusion heterogeneity index (SEM_ α) and distributed diffusion coefficient (SEM_DDC) of SEM; and the mono_ADC, respectively.

Postprocessing and image interpretation

Two board-certified radiologists with 10 and 14 years of experience in gastrointestinal (GI) radiology independently assessed the quality of MR images via the 5-point scale approach. Scores ranging from 1 to 5 indicate poor, mild, average, good and excellent tumor detection and anatomical detail display, respectively, and severe, massive, moderate, mild, and none for observed artifacts or image distortions. Images scored less than 3 by any of the radiologists were excluded from analysis. The raw data were imported to ITK-SNAP (v3.8.0, <http://www.itksnap.org>) for tumor segmentation using a 3D volume of interest (VOI) method. The two radiologists used T2WI as the reference and manually delineated the region of interest (ROI) along the outer boundary of tumor on the axial plane of the b = 800 s/mm² images, and finally integrated all the ROIs into a 3D-VOI (Fig. 2). Thereafter, the data obtained from the six DWI models were uploaded as supplementary data, and the same VOI was duplicated and applied on each DWI model to generate relevant parametric maps (Fig. 3). Subsequently, the corresponding quantitative parameters were automatically computed using the “volume and statistics” function within the “segmentation” toolbar of ITK-SNAP. The interobserver agreement between the two readers’ measurements were performed, and if good agreements were achieved, the mean of their measurements were used for subsequent

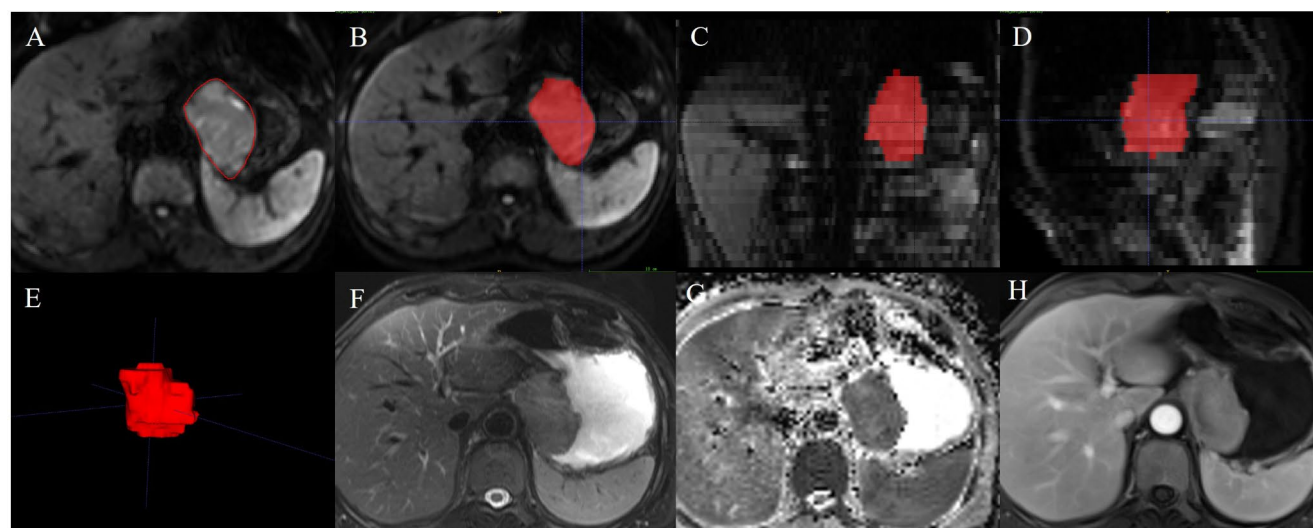


Fig. 2 Diagrams of tumor segmentation process and relevant tumor display on conventional MR images. (A) Tumor segmentation along the outer boundary at the maximal layer on the axial plane; (B) Completed tumor segmentation occupying the whole tumor area on the axial plane; (C) Completed tumor segmentation on the coronal plane;

(D) Completed tumor segmentation on the sagittal plane; (E) Fused 3D volumetric tumor segmentation; (F) Axial fat suppressed T2WI shows a mildly hyperintense tumor in the gastric body; (G) ADC map shows the tumor presents markedly hypointense appearance; (H) Axial contrast-enhanced images

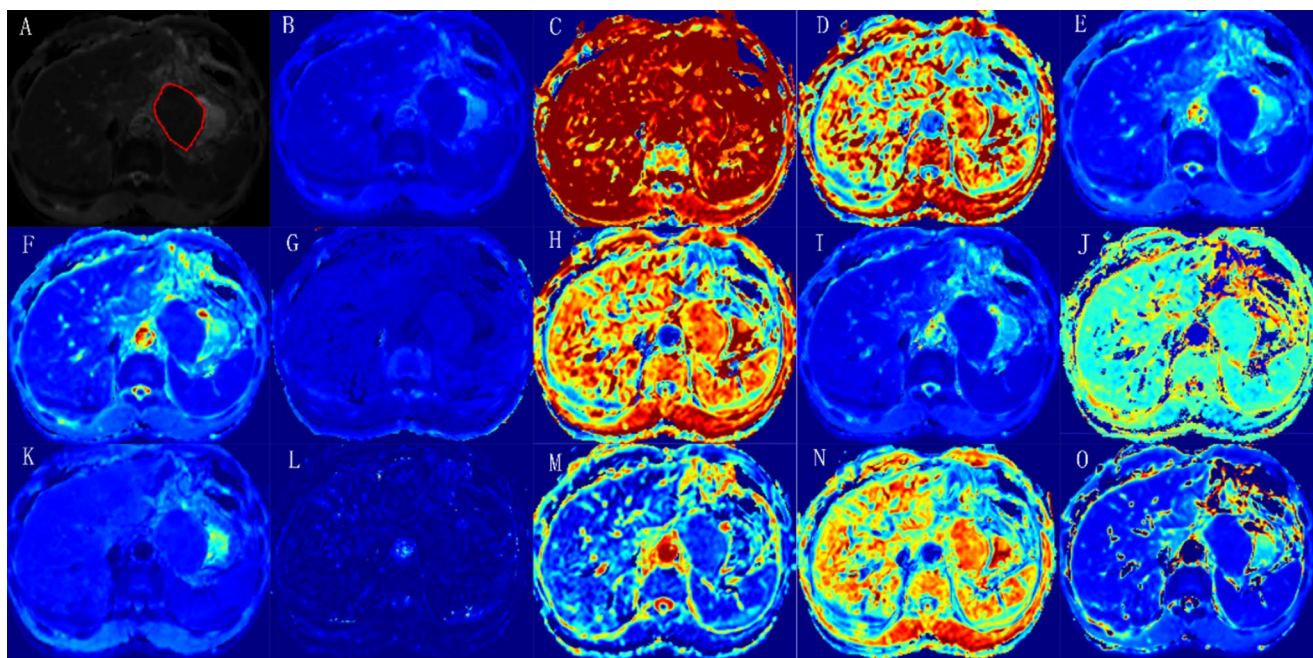


Fig. 3 Parametric maps derived from six diffusion-weighted MRI models in a LNM-positive patients with pathologically confirmed gastric adenocarcinoma by radical gastrectomy, pT3N1M0. (A) Mono_ADC grayscale map with tumor segmentation; (B) Mono_ADC jet map; (C)

CTRW_α map; (D) CTRW_β map; (E) CTRW_D map; (F) DKI_D map; (G) DKI_K map; (H) FROC_β map; (I) FROC_D map; (J) FROC_μ map; (K) IVIM_D map; (L) IVIM_D* map; (M) IVIM_f map; (N) SEM_α map; (O) SEM_DDC map

analysis. Regarding morphologic features, the two radiologists independently interpreted the MR images without knowing the pathological results. We determined tumor thickness based on the maximum diameter perpendicular to the longest axis plane [12]. Clinical staging in this study refers to the local-regional tumor (cT) and node staging (cN). Clinical node staging was classified into cN-positive or negative, described as positive or negative MRI-reported-LN status, following the newly proposed Node-RADS 1.0 scheme [29, 30] and patients were recorded as positive when regional nodes reached Node-RADS score ≥ 3 by any of the radiologist, vice versa. Specifically, cN-positive was determined on T2WI as the presence of a nodal morphologic abnormality (short-axis diameter ≥ 10 mm, round shape, clustering, irregular/spiculated nodal margins, and heterogeneous signal intensity); and on DWI as the presence of restricted signal intensity on $b=800$ s/mm² and hypointense on corresponding ADC maps. Clinical tumor staging refers to tumor infiltration depth (cT1~4a) in this study and were determined according to the 8th edition of the American Joint Commission on Cancer, or AJCC [8] by radiologists' readings on T2WI, DWI and enhanced MRI [12, 14, 25]. Be specific, in this study, T1 tumors regard to invasion depth limited to mucosa or submucosa and present only mildly irregular mucosal abnormality; T2: tumoral infiltration of the muscularis propria which can be identified as focal wall-thickening with or without ulceration; T3: tumoral penetration of the subserosal fat without invasion

of the visceral peritoneum or adjacent structures; and T4a: tumoral invasion of the serosa, peri-gastric fat infiltration or nodular bulging around the tumor can be clearly identified. The final diagnoses were determined by the consensus of the two radiologists, any disagreement was resolved by consulting to a third GI radiologist with 23 years of experience.

Pathologic diagnosis

Post-surgical pathology from 4-μm-thick sections stained with hematoxylin and eosin (HE) were examined by a board-certified pathologist with 9 years of experience in GI pathology, following the diagnostic criteria of the 8th AJCC [8]. Tumor location, histodifferentiation grade, LNM, ulceration status, pathological tumor stage (pT), Lauren subtype, perineural invasion (PNI), and lymphovascular invasion (LVI) were analyzed.

Statistical analysis

The statistical analysis was conducted with Medcalc 18.0. Two-sided $P < 0.05$ indicated statistical significance. The intraclass correlation coefficient (ICC) and 95% confidence intervals (CIs) were used to evaluate inter-reader variability between the measurements of DWI models-derived parameters. The ICC values of 0.00–0.20, 0.21–0.40, 0.41–0.60, 0.61–0.80, and 0.81–1.00 indicated low, fair, moderate, good, and excellent correlations, respectively. Normally

Table 2 Comparison of clinicopathological characteristics between LNM negative and LNM positive groups

Clinicopathological characteristics		Overall (n=58)	LNM (-) (n=16)	LNM (+) (n=42)	$\chi^2/t/Z$ value	<i>P</i> value
Age (years)	Range: 39–77	60.88 ± 10.48	60.94 ± 9.82	60.86 ± 10.83	0.260	0.979
Sex	Male	41	14	27	3.014	0.112
	Female	17	2	15		
Location	Cardia/Fundus	19	4	15	1.634	0.442
	Gastric body	27	7	20		
	Antrum	12	5	7		
Histodifferentiation*	Poor	38	7	31	0.002	
	Moderate	16	5	11		
	Well	4	4	0		
Ulceration	Absent	8	4	4	2.234	0.198
	Present	50	12	38		
pT	1	9	8	1	22.059	<0.001
	2	15	4	11		
	3	17	1	16		
	4a	17	3	14		
Lauren subtype	Intestinal	13	9	4	14.557	0.001
	Mixed	12	2	10		
	Diffuse	33	5	28		
PNI	Negative	23	12	11	11.535	0.001
	Positive	35	4	31		
LVI	Negative	18	13	5	25.031	<0.001
	Positive	40	3	37		

Abbreviations LNM = Lymph node metastasis; (-) = Negative; (+) = Positive; pT = Pathologic tumor stage; PNI = Perineural invasion; LVI = Lymphovascular invasion; Note: Histodifferentiation* means the comparison of this characteristics using Fisher's exact test, no statistic here

distributed data are presented as the mean ± standard deviation ($X \pm s$); otherwise, the data are presented as the median (25th quartile, 75th quartile) [M (Q1, Q3)]. Continuous variables were compared using either the Mann–Whitney *U* test or Student's *t* test. Categorical variables were analyzed using Fisher's exact test or the chi-square test. Multivariable logistic regression was employed to identify independent predictors of LNM. Diagnostic performances were evaluated through the ROC analysis. The area under the curve (AUC), specificity, sensitivity, positive and negative predictive values (PPV/NPV) were calculated. Differences among AUCs were compared using the Delong test. The relationships between DWI parameters and LNM status were evaluated through Spearman's rank correlation test, with *r* values of 0.00–0.20, 0.21–0.40, 0.41–0.60, 0.61–0.80, and 0.81–1.00 indicating low, fair, moderate, good, and excellent correlations, respectively.

Results

Clinicopathological characteristics

Fifty-eight patients were ultimately recruited, including 41 men and 17 women, aged 39–77 (average, 60.88 ± 10.48) years. After surgery, 42 patients were pathologically

confirmed as LNM positive (72.4%), and 16 were LNM negative (27.6%). No evidences of differences were identified in age, sex, location, or ulceration between the two groups (all $P > 0.05$). As depicted in Table 2, significant differences were observed in terms of histodifferentiation, pT, Lauren subtype, LVI, and PNI. Specifically, compared to the LNM-negative group, the LNM-positive group contained more lesions with poor histodifferentiation (31 vs. 7), the diffuse Lauren subtype (28 vs. 5), advanced pT3-4a lesions (30 vs. 4), positive LVI (37 vs. 3), and positive PNI (31 vs. 4).

Comparisons of MRI parameters

The values of DWI models-derived parameters showed good to perfect inter-reader variability, ranging from ICC = 0.815 to ICC = 0.981 (Table S1, Supplementary material).

As shown in Fig. 4; Table 3, the mean tumor thickness was 20.20 ± 6.49 mm in the LNM-positive group, significantly larger than those in the LNM-negative group ($t = 2.345$, $P = 0.023$). Compared with the LNM-negative group, the mean values of CTRW_D, DKI_D, FROC_D, IVIM_D*, and IVIM_f in the LNM-positive group decreased, whereas the mean value of DKI_K significantly increased (all $P < 0.05$). In addition, cT and MRI-reported-LN status were significantly different between the two groups (all $P < 0.05$).

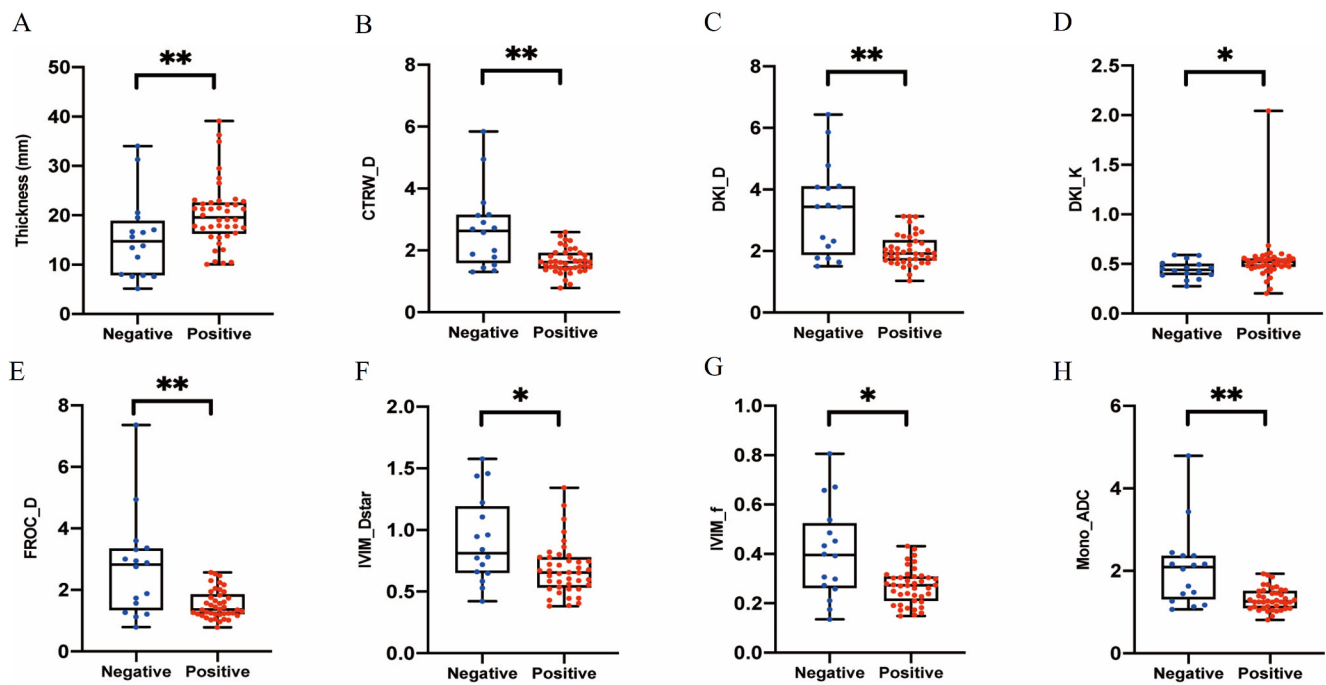


Fig. 4 Box and whisker plots for the comparison of mean values of significant MRI parameters between LNM negative group and LNM positive group. (A) Thickness; (B) CTRW_D; (C) DKI_D, (D) DKI_K; (E) FROC_D; (F) IVIM_D*; (G) IVIM_f; (H) IVIM_ADC

No evidences of differences were observed in CTRW $_{\alpha}$, CTRW $_{\beta}$, FROC $_{\beta}$, FROC $_{\mu}$, IVIM_D, SEM $_{\alpha}$ or SEM_DDC between the two groups.

Independent predictors

Univariable regression analysis showed that cT, MRI-reported-LN, thickness, CTRW_D, DKI_D, DKI_K, FROC_D, IVIM_D*, IVIM_f, Mono_ADC were significant for predicting LNM status. Multivariable logistic regression analysis demonstrated that cT and CTRW_D were independent predictors and used to establish a combined parameter (odds ratio = 3.241, $P = 0.037$, for cT, odds ratio = 0.948, $P = 0.020$, for CTRW_D; Table 4). The Hosmer and Lemeshow test showed good consistency between the probability of LNM positivity predicted by the combined parameter and the actual incidence of LNM positivity ($\chi = 4.648$, $P = 0.794$).

Diagnostic performance

As shown in Fig. 5, the ROC analysis results revealed the combined parameter yielded the highest AUC of 0.930 (95%CI: 0.831, 0.980), significantly higher than the AUCs of cT and CTRW_D ($Z = 2.590$, $P = 0.010$ vs. cT; $Z = 2.149$, $P = 0.032$ vs. CTRW_D). The overall accuracy of MRI-reported-LN was 65.52% with its AUC reached 0.723; compared to surgical pathology, MRI-reported-LN correctly diagnosed 14 true LNM-negative and 24 true

LNM-positive. The combination of CTRW_D and MRI-reported-LN showed a significantly improved performance with AUC being 0.869. Specifically, MRI-reported-LN diagnosed LNM-negative in 32 patients, among whom 18 were pathologically confirmed as LNM-positive; when using $> cT2$ and $CTRW_D \leq 2.467 \times 10^{-3}/mm^2$ as the diagnostic criteria, 17 and 23 were categorized as LNM-positive rather than negative. Compared to pathologic results, cT and CTRW correctly diagnosed 21 and 24 out of these 32 patients with their accuracies reaching 65.63% (21/32) and 75% (24/32), respectively. Furthermore, model-by-model comparison revealed that DWI models demonstrated non-significantly different performances. No evidences of significant differences were identified among AUCs of individual parameters (all $P > 0.05$, Table S2 in Supplementary material). The combined parameter exhibited significantly higher performances than any other parameters and models as shown in Table 5.

Correlations between significant MRI parameters and LNM status

Tumor thickness, cT, MRI-reported-LN status, DKI_K, and the combined parameter were significantly and positively correlated with the LNM status. Inverse correlations were identified between FROC_D, IVIM_D*, IVIM_f, CTRW_D, DKI_D, Mono_ADC, and the LNM status (Table S3, Supplementary material).

Table 3 Comparison of MRI parameters between LNM negative and LNM positive groups

MRI parameters		LNM (-) (n=16)	LNM (+) (n=42)	t/z/ χ^2 value	P value
cT*	1	6	0	-	<0.001
	2	4	8		
	3	6	25		
	4a	2	9		
MR reported LN status	Negative	14	18	9.336	0.002
	Positive	2	24		
Thickness (mm)	Mean: 18.9±7.3 Range: 11–43	15.39±8.20	20.20±6.49	-2.345	0.023
CTRW_α		0.91±0.10	0.88±0.08	1.458	0.150
CTRW_β		0.60±0.14	0.64±0.11	-1.015	0.315
CTRW_D		2.67±1.29	1.65±0.40	3.122	0.007
DKI_D		3.44 (1.87, 4.2)	1.92(1.68, 2.45)	-3.062	0.002
DKI_K		0.44 (0.388, 0.57)	0.52 (0.47, 0.62)	-2.296	0.022
FROC_β		0.65±0.13	0.67±0.14	-0.553	0.582
FROC_D		2.82 (1.34, 3.35)	1.36 (1.21, 1.86)	2.836	0.005
FROC_μ		3.38±0.89	3.43±0.66	-0.221	0.826
IVIM_D		1.01±0.15	0.92±0.15	1.935	0.058
IVIM_D*		0.92±0.35	0.68±0.21	2.546	0.020
IVIM_f		0.41±0.19	0.27±0.72	2.785	0.013
Mono_ADC		2.067±0.96	1.31±0.26	3.096	0.007
SEM_α		0.46±1.07	0.47±1.02	-0.359	0.721
SEM_DDC		2.44±0.72	2.18±0.50	1.573	0.121

Abbreviations LNM=Lymph node metastasis; (-)=Negative; (+)=Positive; ADC=Apparent diffusion coefficient; CTRW=Continuous time random walk diffusion-weighted imaging; CTRW_α=Temporal diffusion heterogeneity; CTRW_β=Spatial diffusion heterogeneity; CTRW_D=Anomalous diffusion coefficient; DKI=Diffusion kurtosis imaging; DKI_D=Diffusivity; DKI_K=Kurtosis; FORC=Fractional order calculus diffusion; FROC_D=Diffusion coefficient; FROC_β=Intravoxel diffusion heterogeneity parameter; FROC_μ=Spatial parameter; IVIM=Intravoxel incoherent motion diffusion-weighted imaging; IVIM_D=True diffusion coefficient; IVIM_D*=Pseudodiffusion coefficient; IVIM_f=Pseudodiffusion fraction; SEM=Stretched exponential model; SEM_α=Water diffusion heterogeneity index; SEM_DDC=Distributed diffusion coefficient

Note: cT* means the comparison of this characteristics using Fisher's exact test, no statistic here. Normally distributed data were presented as mean±standard deviation ($\bar{X}\pm s$), and skewed data were formatted as the median (25% quartile, 75% quartile) [M (Q1, Q3)]

Table 4 Univariable and multivariable regression analysis of MRI parameters for LNM prediction

Variables	Univariable regression analysis		Multivariable regression analysis	
	OR (95% CI) value	P value	OR (95% CI) value	P value
cT	5.786 (2.166, 15.453)	<0.001	3.241 (1.076, 9.761)	0.037
MRI reported LN status	9.333 (1.879, 46.353)	0.006		
Thickness	1.123 (1.012, 1.247)	0.029		
CTRW_D	0.978 (0.967, 0.999)	0.002	0.948 (0.922, 0.998)	0.020
DKI_D	0.998 (0.998, 0.999)	0.001		
DKI_K	1.006 (1.000, 1.012)	0.064		
FROC_D	0.998 (0.998, 0.999)	0.002		
IVIM_D*	0.997 (0.994, 0.999)	0.008		
IVIM_f	0.991 (0.984, 0.997)	0.004		
Mono_ADC	0.997 (0.995, 0.999)	0.001		

Discussion

This work investigated the potential of six advanced DWI models for preoperative prediction of LNM in resectable GC patients. ADC, CTRW_D, DKI_D, DKI_K, FROC_D, IVIM_D*, and IVIM_f demonstrated clinically acceptable performance for LNM prediction. Furthermore, CTRW_D

and cT were independent predictors and used to establish a combined parameter, which further improved the performance. These DWI models offer new sets of imaging markers for depicting tumor characteristics and can serve as useful tools for quantitative prediction of LNM. The mono-exponential diffusion model-derived ADC is useful for distinguishing LN status in GC [31]. The ADC values in the

Fig. 5 Comparison of performances of MRI parameters for predicting LNM in gastric cancer patients. The combined parameter (cT+CTRW_D, the solid purple line) presents the highest AUC of 0.930

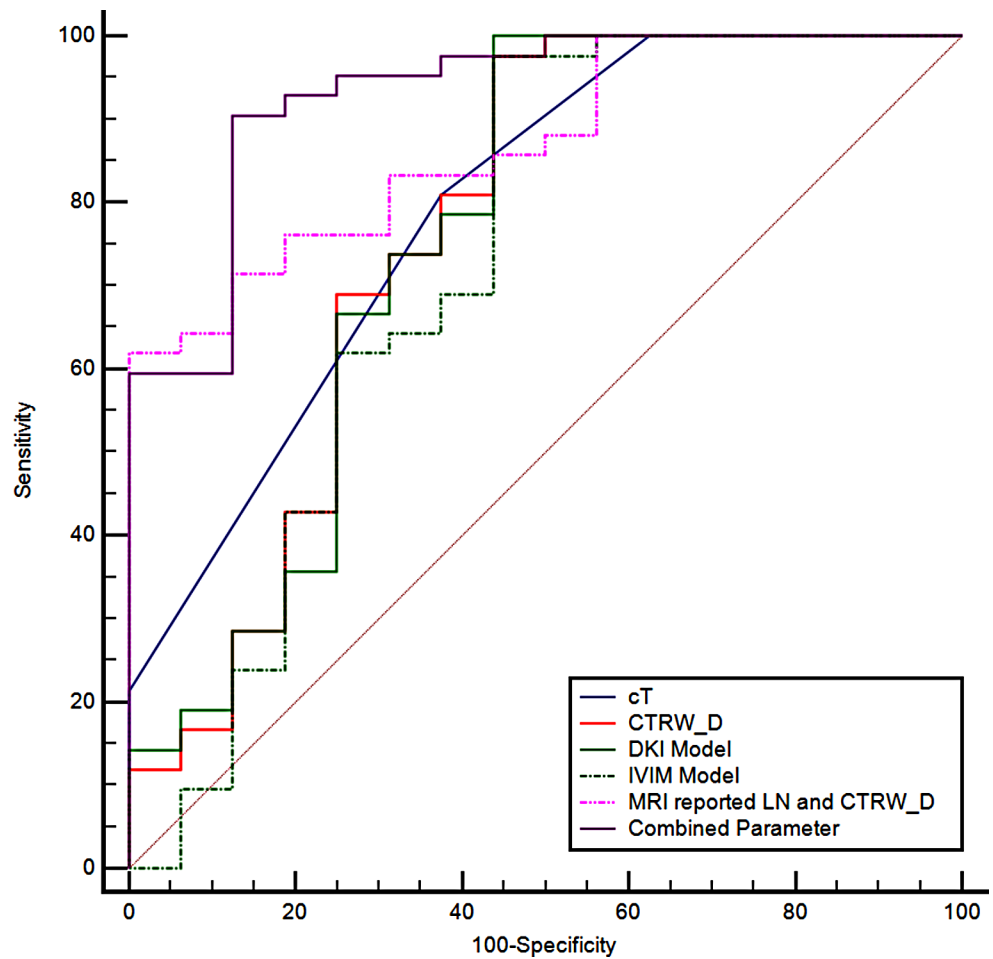


Table 5 Comparison among diagnostic efficacies of MRI parameters in predicting LNM positivity in resectable gastric cancer

Parameters	AUC (95% CI)	Sensitivity	Specificity	Cut off value	Youden index	PPV (% , 95% CI)	NPV (% , 95% CI)	Z value	P value
cT	0.793 (0.659, 0.927)	80.95	62.50	> cT2	0.435	85.00 (70.16, 94.29)	55.56 (30.76, 78.47)	4.704	0.001
CTRW_D	0.767 (0.637, 0.928)	97.62	56.25	≤2.467	0.539	85.41 (72.33, 93.93)	90.01 (55.51, 99.75)	3.876	0.002
CTRW_D+MRI reported LN	0.869 (0.755, 0.94)	61.00	100	>0.837	0.619	100 (86.77, 10)	50 (31.89, 68.11)	7.907	<0.001
DKI model (D+K)	0.760 (0.630, 0.863)	100	56.25	>0.395	0.563	85.71 (72.76, 94.06)	100 (66.38, 100)	3.056	0.002
IVIM model (D*+f)	0.729 (0.596, 0.838)	97.62	56.25	>0.537	0.539	85.41 (72.33, 93.93)	90.01 (55.51, 99.75)	2.490	0.013
Combined parameter	0.930 (0.831, 0.980)	90.48	87.50	>0.663	0.780	95 (83.08, 99.39)	77.79 (52.34, 93.60)	11.477	<0.001

Abbreviations CI=Confidence interval; cT=Clinical stage; PPV=Positive predictive value; NPV=Negative predictive value; ADC=Apparent diffusion coefficient; CTRW_D=Anomalous diffusion coefficient; DKI_D=Diffusivity; FROC_D=Diffusion coefficient; IVIM_D*=Pseudodiffusion coefficient; IVIM_f=Pseudodiffusion fraction

LNM-positive group were significantly lower than those in the LNM-negative group, and the ADC alone demonstrated a similar performance to that reported previously (0.767 vs. 0.788). Shi B et al. reported that DKI_D and DKI_K were correlated with the tumor necrosis fraction after TGF-β1 inhibition in mouse GC models [32]. A lower DKI_D is

suggestive of higher risk of LNM and advanced stage for endometrial carcinoma [33]. DKI_K holds the potential to capture microstructural complexity and heterogeneity [26, 34]. Therefore, DKI_D together with DKI-K can provide insights into tumor aggressiveness and heterogeneity, which may facilitate preoperative identification of LNM. We

found significantly decreased DKI_D and increased DKI_K values in the lesions of LNM-positive group, suggesting the higher levels of heterogeneity in these lesions. $IVIM_f$ is effective for distinguishing different node stages in GC [19], and a prior study has proved that $IVIM_f$ is a useful marker for assessing LVI [25]. GC metastasis to lymph nodes is a complicated process involving disruption of the lymphatic network and neovascularization [35, 36], which may result in an increase in the f value in LNM-positive GC lesions. Based on the previous evidences, $IVIM_D^*$ is not useful for characterizing or staging GC [19, 25]. However, we found a significant reduction of D^* value in the LNM-positive group. According to the $IVIM$ theory, D^* represents microcirculation perfusion of tissues [35]. The reduced D^* value may indicate that GC lesions with positive LNM have less perfusion than those without LNM; nevertheless, this was a preliminary result that needs further validation. $CTRW$ was firstly applied in the brain for characterizing both degenerative diseases and gliomas [37, 38] and has been utilized for solid tumors such as breast cancer recently [39]; nevertheless, no study has ever applied $CTRW$ in the stomach. Our preliminary results showed that GC lesions with positive LNM had lower $CTRW_D$ values than those without LNM. Moreover, $CTRW_D$ exhibited superior performance compared to the other parameters and emerged as one of the risk factors of LNM. Lower $CTRW_D$ were closely associated with more advanced disease stages [38, 39]. Tumors with advanced stage are of high cellularity, leading to reduced extracellular space and lower $CTRW_D$ values [39]. However, in this study, we failed to prove the usefulness of the α and β parameters for predicting LNM, which were contrary to a previous report [36]. This discrepancy may attribute to the variations in sample size, different types of cancers; the choice of b values for sequence acquisition may be another possible reason. The FROC has been applied to classify the Lauren subtype in GC [27]. The derived β , D , and μ_1 parameters exhibited favorable performance for distinguishing the intestinal-and-mixed subtypes from the diffuse subtypes. Besides, previous studies have proved close and inverse likelihood between D values and significant prognostic histologic markers of LVI and LNM [25, 31]; consistently, negative correlations were identified between D values and LNM status in this study. β is related to intravoxel diffusion heterogeneity, and μ_1 is linked to the diffusion mean free length and cellularity [27]. Theoretically, these factors together reflect tumor cellularity heterogeneity and may vary between patients with different LNM status. However, no significant differences in β or μ_1 were observed in this study. The possible reasons may due to the small sample size and b values adopted for DWI acquisition. Regarding morphologic MRI features, cT outweighed others and were a predictor of LNM. cT is

the standard of care in clinical practice and closely associated with LNM [12, 19]. We found that cT and $CTRW_D$ have overweighted MRI-reported-LN and exhibited added value in MRI-reported-LN negative cohort. Besides, combining $CTRW_D$ with MRI-reported-LN exhibited significantly better performance compared to MRI-reported-LN alone, suggesting quantitative $CTRW_D$ has incremental benefit on this issue. Furthermore, the combination of cT and $CTRW_D$ demonstrated a more favorable performance, underscoring the feasibility and superiority of integrating both qualitative and quantitative parameters from a single MRI scan for GC patients. Certain limitations should be noted in this study. First, the sample size was small, and the results were preliminary; therefore, further researches are needed. Second, mixed adenocarcinomas were eliminated from the analysis since they may cause migration and bias in ADC values calculations. Third, the standard scanning specification for multi- b value DWI lacks global consensus, our results were generated from the sequence with the maximal b -value at 3000 s/mm^2 which may not be applicable to other cancers. In conclusion, the proposed six DWI models offer new sets of quantitative imaging markers for preoperative prediction of LNM in resectable GC, with $CTRW_D$ appearing as the most beneficial marker. The combination of $CTRW_D$ and cT demonstrates significant added value and further enhances the predictive performance.

Supplementary Information The online version contains supplementary material available at <https://doi.org/10.1007/s00261-024-04559-3>.

Author contributions Guarantor: Jinrong Qu; Conceptualization: Jing Li, Jinrong Qu; data curation: Yi Wang, Fei Ma, and Hongkai Zhang; formal analysis: Jing Li, Tianxia Bei, and Shaoxu Wang; investigation: Jing Li, Tianxia Bei, Yi Wang, and Fei Ma; methodology and statistical analysis, Haocheng Li, Shaoxu Wang; supervision, Jinrong Qu; writing—original draft, all authors; writing—review and editing, all authors.

Funding This study has received funding from Special funding of the Henan Health Science and Technology Innovation Talent Project (YXKC2021054), National Natural Science Foundation of China (82202146, 8227071914), Science and Technology Development Foundation of Henan Province (242102311173).

Data availability No datasets were generated or analysed during the current study.

Declarations

Competing interests The authors declare no competing interests.

References

1. Bray F, Laversanne M, Sung H et al. (2024) Global cancer statistics 2022: GLOBOCAN estimates of incidence and mortality worldwide for 36 cancers in 185 countries. *CA Cancer J Clin* 74:229–263. doi: <https://doi.org/10.3322/caac.21834>.
2. Smyth EC, Nilsson M, Grabsch HI et al. (2020) Gastric cancer. *Lancet* 396: 635–648. doi: [https://doi.org/10.1016/S0140-6736\(20\)31288-5](https://doi.org/10.1016/S0140-6736(20)31288-5).
3. Zhang P, Xu T, Feng H et al. (2023) Risk of lymph node metastasis and feasibility of endoscopic submucosal dissection in undifferentiated-type early gastric cancer. *BMC Gastroenterol* 23:175. doi: <https://doi.org/10.1186/s12876-023-02771-x>.
4. Hwang JE, Kim H, Shim HJ et al. (2019) Lymph-node ratio is an important clinical determinant for selecting the appropriate adjuvant chemotherapy regimen for curative D2-resected gastric cancer. *J Cancer Res Clin Oncol* 145:2157–2166. doi: <https://doi.org/10.1007/s00432-019-02963-7>.
5. Sinnamon AJ, Savoldy M, Mehta R et al. (2023) Tumor Regression Grade and Overall Survival following Gastrectomy with Preoperative Therapy for Gastric Cancer. *Ann Surg Oncol* 30:3580–3589. doi: <https://doi.org/10.1245/s10434-023-13151-w>.
6. Yamashita K, Hosoda K, Ema A. (2016) Lymph node ratio as a novel and simple prognostic factor in advanced gastric cancer. *Eur J Surg Oncol* 42:1253–1260. doi: <https://doi.org/10.1016/j.ejso.2016.03.001>.
7. Toriumi T, Terashima M, Mizusawa J et al. (2023) Recurrence patterns after curative gastrectomy for pStage II/III gastric cancer: Exploratory analysis of the randomized controlled JCOG1001 trial. *Eur J Surg Oncol* 49:838–844. doi: <https://doi.org/10.1016/j.ejso.2022.11.093>.
8. College of American Pathologists. Protocol for the examination of specimens from patients with carcinoma of the stomach (Version: Stomach 4.1.0.0) [EB/OL]. <https://documents.cap.org/protocols/cp-giupper-stomach-20-4100.pdf>. Published February 2020. Accessed November 2020.
9. Ajani JA, D'Amico TA, Bentrem DJ et al. (2022) Gastric Cancer, Version 2.2022, NCCN Clinical Practice Guidelines in Oncology. *J Natl Compr Canc Netw* 20:167–192. doi: <https://doi.org/10.6004/jnccn.2022.0008>.
10. Saito T, Kurokawa Y, Takiguchi S et al. (2015) Accuracy of multidetector-row CT in diagnosing lymph node metastasis in patients with gastric cancer. *Eur Radiol* 25:368–374. doi: <https://doi.org/10.1007/s00330-014-3373-9>.
11. Wei J, Zhang Y, Wang Z et al. (2021) Identification of lymph node metastasis by computed tomography in early gastric cancer. *Chin J Cancer Res* 33:671–681. doi: <https://doi.org/10.21147/j.issn.1000-9604.2021.06.04>.
12. Li J, Fang M, Wang R et al. (2018) Diagnostic accuracy of dual-energy CT-based nomograms to predict lymph node metastasis in gastric cancer. *Eur Radiol* 28: 5241–5249. doi: <https://doi.org/10.1007/s00330-018-5483-2>.
13. Lin R, Lin Z, Chen Z et al. (2022) ⁶⁸Ga-DOTA-FAPI-04 PET/CT in the evaluation of gastric cancer: comparison with ¹⁸F-FDG PET/CT. *Eur J Nucl Med Mol Imaging* 49:2960–2971. doi: <https://doi.org/10.1097/RLU.0000000000004073>.
14. Withey SJ, Goh V, Foley KG. (2022) State-of-the-art imaging in oesophago-gastric cancer. *Br J Radiol* 95:20220410. doi: <https://doi.org/10.1259/bjr.20220410>.
15. Arslan H, Fatih Özbay M, Çallı İ et al. (2017) Contribution of diffusion weighted MRI to diagnosis and staging in gastric tumors and comparison with multi-detector computed tomography. *Radiol Oncol* 51:23–29. doi: <https://doi.org/10.1515/raon-2017-0002>.
16. Giganti F, Ambrosi A, Chiari D et al. (2017) Apparent diffusion coefficient by diffusion-weighted magnetic resonance imaging as a sole biomarker for staging and prognosis of gastric cancer. *Chin J Cancer Res* 29:118–126. doi: <https://doi.org/10.21147/j.issn.1000-9604.2017.02.04>.
17. Le Bihan D. (2013) Apparent diffusion coefficient and beyond: what diffusion MR imaging can tell us about tissue structure. *Radiology* 268:318–322. doi: <https://doi.org/10.1148/radiol.13130420>.
18. Yuan L, Lin X, Zhao P et al. (2023) Correlations between DKI and DWI with Ki-67 in gastric adenocarcinoma. *Acta Radiol* 64:1792–1798. doi: <https://doi.org/10.1177/02841851231153035>.
19. Zeng Q, Hong Y, Cheng J et al. (2021) Quantitative study of preoperative staging of gastric cancer using intravoxel incoherent motion diffusion-weighted imaging as a potential clinical index. *Eur J Radiol* 141:109627. doi: <https://doi.org/10.1016/j.ejrad.2021.109627>.
20. Lin M, Yu X, Chen Y et al. (2017) Contribution of mono-exponential, bi-exponential and stretched exponential model-based diffusion-weighted MR imaging in the diagnosis and differentiation of uterine cervical carcinoma. *Eur Radiol* 27:2400–2410. doi: <https://doi.org/10.1007/s00330-016-4596-8>.
21. Karaman MM, Wang H, Sui Y et al. (2016) A fractional motion diffusion model for grading pediatric brain tumors. *Neuroimage Clin* 12:707–714. doi: <https://doi.org/10.1016/j.nicl.2016.10.003>.
22. Sui Y, Wang H, Liu G et al. (2015) Differentiation of Low- and High-Grade Pediatric Brain Tumors with High b-Value Diffusion-weighted MR Imaging and a Fractional Order Calculus Model. *Radiology* 277:489–496. doi: <https://doi.org/10.1148/radiol.2015142156>.
23. Yu Q, Reutens D, O'Brien K et al. (2017) Tissue microstructure features derived from anomalous diffusion measurements in magnetic resonance imaging. *Hum Brain Mapp* 38:1068–1081. doi: <https://doi.org/10.1002/hbm.23441>.
24. Tang L, Sui Y, Zhong Z et al. (2018) Non-Gaussian diffusion imaging with a fractional order calculus model to predict response of gastrointestinal stromal tumor to second-line sunitinib therapy. *Magn Reson Med* 79:1399–1406. doi: <https://doi.org/10.1002/mrm.26798>.
25. Li J, Yan LL, Zhang HK et al. (2023) Application of intravoxel incoherent motion diffusion-weighted imaging for preoperative knowledge of lymphovascular invasion in gastric cancer: a prospective study. *Abdom Radiol (NY)* 48:2207–2218. doi: <https://doi.org/10.1007/s00261-023-03920-2>.
26. Fu J, Tang L, Li ZY et al. (2020) Diffusion kurtosis imaging in the prediction of poor responses of locally advanced gastric cancer to neoadjuvant chemotherapy. *Eur J Radiol* 128:108974. doi: <https://doi.org/10.1016/j.ejrad.2020.108974>.
27. Karaman MM, Tang L, Li Z et al. (2021) In vivo assessment of Lauren classification for gastric adenocarcinoma using diffusion MRI with a fractional order calculus model. *Eur Radiol* 31:5659–5668. doi: <https://doi.org/10.1007/s00330-021-07694-3>.
28. Koh DM, Collins DJ, Orton MR (2011) Intravoxel incoherent motion in body diffusion-weighted MRI: reality and challenges. *AJR Am J Roentgenol* 196:1351–1361. doi: <https://doi.org/10.2214/AJR.10.5515>.
29. Elsholtz FHJ, Asbach P, Haas M et al. (2021) Introducing the Node Reporting and Data System 1.0 (Node-RADS): a concept for standardized assessment of lymph nodes in cancer. *Eur Radiol* 31:6116–6124. doi: <https://doi.org/10.1007/s00330-020-07572-4>.
30. Loch FN, Beyer K, Kreis ME et al. (2023) Diagnostic performance of Node Reporting and Data System (Node-RADS) for regional lymph node staging of gastric cancer by CT. *Eur Radiol* 34:3183–3193. doi: <https://doi.org/10.1007/s00330-023-10352-5>.
31. Liu S, Wang H, Guan W et al. (2015) Preoperative apparent diffusion coefficient value of gastric cancer by diffusion-weighted

- imaging: Correlations with postoperative TNM staging. *J Magn Reson Imaging* 42:837–843. doi: <https://doi.org/10.1002/jmri.24841>.
32. Shi B, Yuan F, Yan F et al. (2019) Evaluation of Effects of TGF- β 1 Inhibition on Gastric Cancer in Nude Mice by Diffusion Kurtosis Imaging and In-Line X-ray Phase Contrast Imaging With Sequential Histology. *J Magn Reson Imaging* 49:1553–1564. doi: <https://doi.org/10.1002/jmri.26523>.
 33. Yamada I, Sakamoto J, Kobayashi D et al. (2019) Diffusion kurtosis imaging of endometrial carcinoma: Correlation with histopathological findings. *Magn Reson Imaging* 57:337–346. doi: <https://doi.org/10.1016/j.mri.2018.12.009>.
 34. Jensen JH, Helpert JA (2010) MRI quantification of non-Gaussian water diffusion by kurtosis analysis. *NMR Biomed* 23:698–710. doi: <https://doi.org/10.1002/nbm.1518>.
 35. Le Bihan D, Turner R (1992) The capillary network: a link between IVIM and classical perfusion. *Magn Reson Med* 27:171–178. doi: <https://doi.org/10.1002/mrm.1910270116>.
 36. Fischbein NJ, Noworolski SM, Henry RG et al. (2003) Assessment of metastatic cervical adenopathy using dynamic contrast-enhanced MR imaging. *AJNR Am J Neuroradiol* 24:301–311.
 37. Gatto RG, Ye AQ, Colon-Perez L et al. (2019) Detection of axonal degeneration in a mouse model of Huntington's disease: comparison between diffusion tensor imaging and anomalous diffusion metrics. *MAGMA* 32:461–471. doi: <https://doi.org/10.1007/s10334-019-00742-6>.
 38. Karaman MM, Zhang J, Xie KL et al. (2021) Quartile histogram assessment of glioma malignancy using high b-value diffusion MRI with a continuous-time random-walk model. *NMR Biomed* 34: e4485. doi: <https://doi.org/10.1002/nbm.4485>.
 39. Qin Y, Tang C, Hu Q et al. (2023) Assessment of Prognostic Factors and Molecular Subtypes of Breast Cancer With a Continuous-Time Random-Walk MR Diffusion Model: Using Whole Tumor Histogram Analysis. *J Magn Reson Imaging* 58:93–105. doi: <https://doi.org/10.1002/jmri.28474>.

Publisher's note Springer Nature remains neutral with regard to jurisdictional claims in published maps and institutional affiliations.

Springer Nature or its licensor (e.g. a society or other partner) holds exclusive rights to this article under a publishing agreement with the author(s) or other rightsholder(s); author self-archiving of the accepted manuscript version of this article is solely governed by the terms of such publishing agreement and applicable law.